Cell Communication and Signaling

RESEARCH

Open Access

Exercise alleviates hematopoietic stem cell injury following radiation via the carnosine/Slc15a2-p53 axis

Hao Zeng[1†], Naicheng Chen[1†], Fang Chen[1], Xiaoyi Zhong[3], Lijing Yang[1], Yukai Lu[1], Mo Chen[1], Mingqiang Shen[1], Song Wang[1], Shilei Chen[1], Jia Cao[4], Xi Zhang[5], Jinghong Zhao[3], Yang Xu[1], Junping Wang[1*] and Mengjia Hu[1,2*]

Abstract

Ionizing radiation (IR) can cause severe dysfunction of hematopoietic stem cells (HSCs), leading to acute or prolonged myelosuppression. In recent years, physical exercise has been recognized as a healthy lifestyle as it can fight a variety of diseases. However, whether it provides protection against IR is not fully understood. In this study, we revealed that long-term moderate exercise mitigated IR-induced hematopoietic injury by generating carnosine from skeletal muscles. We found that exercised mice displayed reduced loss of HSC number and function after IR, accompanied by alleviated bone marrow damage. Interestingly, these effects were largely abrogated by specific deletion of carnosine synthase Carns1 in skeletal muscles. In contrast, carnosine treatment protected HSCs against IR-induced injury. Mechanistically, we demonstrated that exercise-generated carnosine was specifically transported to HSCs via Slc15a2 and then inhibited p53 transcriptional activity by directly interacting with its core DNA-binding domain, which led to downregulation of the p53 target genes p21 and Puma, thus promoting the proliferation and survival and inhibiting the senescence of irradiated HSCs. More importantly, a similar role of the carnosine/Slc15a2-p53 axis was observed in human cord blood-derived HSCs. Collectively, our data reveal that moderate exercise or carnosine supplementation may be potential antiradiation strategies.

Keywords Hematopoietic stem cell, Radiation, Exercise, Carnosine, p53 activity, Senescence

†Hao Zeng and Naicheng Chen contributed equally to this work.

*Correspondence:
Junping Wang
wangjunping@tmmu.edu.cn
Mengjia Hu
humengjia3260@163.com; humengjia@tmmu.edu.cn
[1]State Key Laboratory of Trauma and Chemical Poisoning, Institute of Combined Injury, Chongqing Engineering Research Center for Nanomedicine, College of Preventive Medicine, Third Military Medical University, Chongqing 400038, China
[2]Chinese PLA Center for Disease Control and Prevention, Beijing 100071, China
[3]Department of Nephrology, the Key Laboratory for the Prevention and Treatment of Chronic Kidney Disease of Chongqing, Xinqiao Hospital, Kidney Center of PLA, Third Military Medical University, Chongqing 400037, China
[4]Institute of Toxicology, College of Preventive Medicine, Third Military Medical University, Chongqing 400038, China
[5]Medical Center of Hematology, Xinqiao Hospital, Third Military Medical University, Chongqing 400037, China

Introduction

Hematopoietic stem cells (HSCs), as the most primitive cells in the hierarchy, are responsible for sustaining the hematopoietic homeostasis throughout life [1, 2]. Under normal circumstances, most primitive HSCs are located in the endosteal niche and are retained in a dormant state, which is required to avoid exhaustion of the stem cell pool [3, 4]. After the occurrence of hematopoietic stresses, HSCs are rapidly activated to meet the body's demand for blood cells [5, 6]. However, they may lose regenerative capacity when subjected to strong factors, such as high doses of ionizing radiation (IR) [7, 8]. As proposed, DNA damage induced by IR can trigger a series of biological reactions, including cell cycle arrest, apoptosis and senescence, in HSCs, resulting in acute bone marrow (BM) failure or long-term hematopoietic dysfunction [9, 10]. Given the current increasing risk of nuclear exposure, novel measures to effectively prevent hematopoietic failure following IR are urgently needed.

Overwhelming evidence has revealed that physical exercise has a wide range of beneficial effects on health [11, 12]. Moderate rather than intense exercise not only promotes muscle adaptation in terms of morphology and function, but also improves the functions of other tissues, including the liver, blood vessels, gastrointestinal tract, and immune system [12, 13]. In particular, endurance exercise can maintain the homeostasis of multiple tissues by inhibiting stem cell dysfunction [14]. In recent years, exercise has been shown to influence the hematopoiesis, which mainly involves relatively activated hematopoietic progenitor cells located in the vascular niche [15, 16]. However, the primitive HSCs are still uninfluenced by exercise at steady state [16, 17].

Exercise is a crucial strategy for improving the ability of the body to fight various stresses [18, 19]. Notably, clinical data have shown that moderate exercise provides protection against the side effects of radiation therapy [20]. Consistent with these findings, hematopoietic cells from exercised mice display reduced damage after exposure to IR [21, 22]. Exercise can increase bone mass and mineral density, which may affect the BM niche [22, 23]. Additionally, skeletal muscle is an endocrine organ that secretes soluble factors, namely, myokines [24]. However, how exercise elicits potential effects on hematopoiesis in the context of radiation is poorly understood.

In the present study, we found that moderate exercise alleviated both acute and long-term myelosuppression following IR exposure, which was mainly mediated by skeletal muscle-derived carnosine. Further investigation revealed that carnosine relieved HSC injury after IR via the transporter Slc15a2. Mechanistically, carnosine inhibited the transcriptional activity of p53 through direct binding to the p53 protein, which promoted the proliferation and survival of irradiated HSCs. Importantly, a strong radioprotective role of carnosine in HSCs from human cord blood (CB) was also determined. Overall, carnosine was showed to safeguard HSCs from IR-induced injury, and could serve as a potential radioprotectant for clinical use.

Materials and methods

Animals Normal wild-type mice were obtained from Laipite Biotechnology Company (Chongqing, China). Carns1$^{flox/flox}$/HSA-Cre mice were generated by crossing Carns1$^{flox/flox}$ mice (Cyagen Biosciences Inc, Suzhou, China) with HSA-Cre mice (Cyagen Biosciences Inc), and the global depletion of Carns1 was induced by injecting the mice with 75 mg/kg tamoxifen (Sigma, St. Louis, MO, USA) for 5 consecutive days. Slc15a2$^{flox/flox}$/Mx1-Cre mice were generated by crossing Slc15a2$^{flox/flox}$ mice (Cyagen Biosciences Inc) with Mx1-Cre mice (Shanghai Model Organisms Center, Shanghai, China), and the deletion of Slc15a2 in the hematopoietic system was induced after intraperitoneal injection of polyinosinic: polycytidylic acid (pIpC) (Sigma), according to our previously published protocol [25]. The p53$^{-/+}$ mice were purchased from Biocytogen Co., Ltd (Beijing, China), and the CD45.1 mice were kindly provided by Prof. Jinyong Wang. All mice used in this study were male, C57BL/6J background, and 6–8 weeks old. The experiments were performed with the approval of the Animal Care Committee of Third Military Medical University.

Exercise A long-term exercise mouse model was established using a small animal treadmill (SA101B; SANS Biotechnology Co., Ltd, Jiangsu, China). The exercise protocol was as follows: after 3 days of acclimation to treadmill running, the mice were allowed to run with no inclination for 65 min/day, once every other day, at a speed of 11.5 m/min. All the mice were exercised for 12 weeks, and age-matched sedentary mice served as controls.

Radiation The cells were irradiated at a dose of 2.0 Gy using an X-ray biological irradiator (X-Rad 320; PXI, North Branford, CT, USA). The mice were subjected to 2.25, 5.0, 8.0 or 10.0 Gy total body irradiation using a ^{60}Co irradiator (Third Military Medical University Irradiation Center).

Carnosine or Nutlin-3a treatment The mice received saline or carnosine (10, 50, 100 or 200 mg/kg) via intraperitoneal injection once a day for 3 days. Within an hour of the last injection, the mice were subjected to IR, and then administered the same dose of carnosine for another 7 days. Nutlin-3a (MedChemExpress, Monmouth Junction, NJ, USA) was intraperitoneally injected into the mice at a dose of 20 mg/kg immediately after IR.

Isolation of human CB CD34$^+$ cells CD34$^+$ cells were purified from human CB using a Human CD34 Positive Selection Kit (Stem Cell Technologies, Vancouver, Canada) according to the manufacturer's instructions. The cells were then used for further experiments, including flow cytometric sorting of hematopoietic stem and progenitor cell (HSPC) populations and lentiviral transfection. CB samples were obtained from the First Affiliated Hospital of Third Military Medical University and informed consent was obtained from all donors. The study was authorized by the institutional review board of the First Affiliated Hospital of Third Military Medical University.

Human CB CD34$^+$ cell culture CD34$^+$ cells transfected with shCtrl or shSLC15A2 were cultured in StemSpan SFEM (Stem Cell Technologies) supplemented with 20 ng/mL human TPO (PeproTech, Rocky Hill, NJ, USA), 100 ng/mL human SCF (PeproTech), 100 ng/mL human Flt3L (PeproTech), 20 ng/mL human IL-6 (PeproTech) and 1× penicillin/streptomycin (Beyotime Biotechnology, Shanghai, China). After culturing at 37 °C for 10 days, the cells were collected for further experiments.

Colony formation assay A total of 3×10^2 LT-HSCs freshly sorted from the BM of irradiated mice treated with saline or carnosine were seeded in MethoCult™ GF M3434 medium (Stem Cell Technologies). After 14 days of culture, the colonies were counted under an inverted microscope.

Flow cytometry To analyze the hematopoietic phenotype in mice, nucleated cells from the BM or peripheral blood (PB) were stained with the following monoclonal antibodies: lineage cocktail (CD3e, Mac-1, Gr-1, B220 and Ter-119), Sca-1, c-Kit, Flk2, CD34, CD150, CD48, CD127, CD16/32, Mac-1, Gr-1, CD3e, B220, CD45.1 and CD45.2. To analyze the hematopoietic phenotype in humans, CB-derived cells were stained with the following monoclonal antibodies: lineage cocktail (CD3, CD14, CD16, CD19, CD20 and CD56), CD38, CD34, CD45RA, CD90, CD33, CD19 and CD45. The cell cycle, in vivo 5-bromodeoxyuridine (BrdU) incorporation, apoptosis and intracellular protein staining analyses were conducted after incubation with the above surface markers, as we have previously described [26, 27]. The samples were detected with a FACSVerse or FACSCanto flow cytometer (BD Biosciences, San Jose, CA, USA), and cell sorting was conducted by a FACSAriaIII sorter (BD Biosciences). The data were analyzed using a FlowJo10.0 software (TreeStar, San Carlos, CA, USA). The antibodies used in the present study were purchased from eBioscience (San Diego, CA, USA) or BioLegend (San Diego), and the details of the antibodies used are provided in Supplementary Table S1.

Competitive transplantation assays A total of 5×10^2 LT-HSCs purified from the BM of control (Ctrl) mice or mice treated with saline or carnosine after IR, together with 5×10^5 CD45.1 BM cells, were transplanted into lethally irradiated (10.0 Gy) CD45.1 recipients through intravenous injection. Sixteen weeks later, 1×10^6 BM cells from primary recipients were transplanted into lethally irradiated (10.0 Gy) CD45.1 recipients. At the indicated times after primary and secondary transplantation, the chimerism and lineage distribution in the PB or BM of recipients were analyzed by flow cytometry.

Xenotransplantation assay Human CB CD34$^+$ cells transfected with shCtrl or shSLC15A2 were exposed to 2.0 Gy IR in the presence of vehicle or carnosine. After being cultured for 10 days, CD34$^+$ CD38$^-$ cells (1×10^3) were sorted and then transplanted into 2.25 Gy-irradiated immunodeficient (M-NSG) mice (Shanghai Model Organisms Center). Sixteen weeks later, the chimerism and lineage distribution of hCD45$^+$ cells in the BM of recipient mice were analyzed by flow cytometry.

Lentiviral transfection CB CD34$^+$ cells were transfected with lentivirus carrying shCtrl or SLC15A2, as described in our previous article [27]. The transduced cells (mCherry$^+$) were subsequently purified via flow cytometry and used for further experiments. All lentiviruses were purchased from Hanbio Co., Ltd. (Shanghai, China). The sequences of the shRNAs are provided in Supplementary Table S2.

Carnosine concentration measurement The carnosine concentration in the serum and BM extracellular fluid (ECF) of the mice was determined using a high-performance liquid chromatography (HPLC) system, as reported previously [28].

Quantitative PCR (qPCR) The relative mRNA expression of the genes mentioned in this study was detected using a CFX96 real-time PCR platform (Bio-Rad, CA, USA) as we have previously reported [27]. The sequences of the primer used are listed in Supplementary Tables S3 and S4.

Western blotting Mouse soleus muscle samples, LSKs (pooled from 7 to 8 mice) or human CD34$^+$ CB cells were lysed in RIPA buffer, and separated by SDS-PAGE followed by incubation with anti-MYH1/2 (Abcam, Cambridge, UK), anti-GAPDH (Invitrogen, Carlsbad, CA, USA), anti-p53 (Abcam), anti-p-p53 (Ser15) (Invitrogen), anti-p21 (Abcam), anti-Puma (Invitrogen), SLC15A2 (Novus, Colorado, USA) or anti-β-actin (Cell Signaling Technology, Danvers, MA, USA). The details of the antibodies used are provided in Supplementary Table S1.

Citrate synthase activity assay The tissue homogenate supernatant samples were obtained from the soleus muscles of mice. Then, citrate synthase activity was detected using the citrate synthase assay kit (Sigma) following the manufacturer's protocol.

RNA sequencing (RNA-seq) LT-HSCs were freshly sorted from the BM of unirradiated or irradiated mice treated with saline or carnosine, followed by immediate isolation of total RNA. After quality control, the sequencing was performed at Sinotech Genomics Co., Ltd. (Shanghai, China). The differentially expressed genes (DEGs) were screened based on the criteria of a fold change > 1.5 and a q-value < 0.05 and are represented in a volcano plot. Gene set enrichment analysis (GSEA) was performed as we described previously [4]. All the raw data have been uploaded to the Gene Expression Omnibus (GEO) database (no. GSE252894 and no. GSE281040).

Chromatin immunoprecipitation (ChIP) This assay was performed according to our previous report [27]. Briefly, Lin^- c-Kit^+ $Sca1^+$ cells (LSKs) were first isolated from the BM of irradiated mice treated with saline or carnosine. The binding of p53 to the promoter regions of Cdkn1a and Bbc3 was subsequently analyzed with a NovoNGS® CUT&Tag 2.0 High-Sensitivity Kit (Novoprotein Scientific, Inc., Shanghai, China) according to the manufacturer's instructions. The antibodies and sequences of the primers used are listed in Supplementary Tables S1 and S5, respectively.

Molecular docking The binding affinity of carnosine for p53 was analyzed using AutoDock Vina software 1.5.6 (Scripps Research Institute, La Jolla, CA, USA). In brief, the protein structure of p53 was acquired through homologous modeling, and the carnosine structure was obtained from the PubChem database. The protein and small molecules were then prepared through the addition of hydrogens, charges and solvation parameters, using AutoDock Tools, followed by a docking procedure. The optimal binding conformation was selected based on the lowest binding energy for analysis of the interaction model and binding sites.

Surface plasmon resonance (SPR) The SPR assay was performed according to the manufacturer's instructions. Briefly, recombinant p53 protein was immobilized onto a CM5 sensor chip (GE Healthcare, Uppsala, Sweden). A range of carnosine concentrations was subsequently flowed through the chip. The binding of carnosine with p53 was tested using a Biacore T200 system (GE Healthcare).

Statistical analysis Differences between two groups were compared using a Student's t test, and one-way analysis of variance (ANOVA) followed by Tukey's post hoc test was used to determine differences among multiple groups. The survival rates of the mice in multiple groups were calculated using the pairwise log-rank test. All data were analyzed with GraphPad Prism 8.0.0 (La Jolla, CA, USA) or SPSS 22.0 (IBM, Chicago, USA) and are presented as mean ± standard deviation (SD). A $p < 0.05$ was defined as the threshold for a statistically significant difference.

Results

Long-term moderate exercise alleviates IR-induced hematopoietic injury in mice

To systematically assess the radioprotective effects of physical exercise, we established a mouse model of long-term treadmill running (Fig. 1A; Supplementary Figure S1A). The improved muscle function in mice after exercise was confirmed by varying degrees of elevation in levels of myosin heavy chain and citrate synthase activity (Supplementary Figures S1B, C). Consistent with the previous report [17], exercised mice did not exhibit significant changes in hematopoietic phenotypes and functions at steady state (Supplementary Figures S1D-I). Interestingly, exercise promoted the recovery of white blood cells (WBCs), red blood cells (RBCs) and platelets (PLTs) in the PB of mice after exposure to 5.0 Gy IR (Fig. 1B-D). Considering that the differences between the two groups were greatest on day 15 after IR, a critical period for hematopoietic regeneration, we focused on this time point for subsequent analyses. Compared with sedentary controls, exercised mice presented an increased number of total BM cells after IR (Fig. 1E; Supplementary Figure S1J). In particular, using flow cytometric analysis, we found that exercise attenuated the loss of LSKs and myeloid progenitors (MPs) in the BM of irradiated mice (Fig. 1F, G). Further analysis revealed that the numbers of all three LSK subpopulations, including long-term HSCs (LT-HSCs), short-term HSCs (ST-HSCs) and multipotent progenitors (MPPs), as well as various lineage-committed progenitors were greater in exercised mice after IR (Fig. 1F, H; Supplementary Figures S1K, L). More importantly, an increased survival rate was observed in exercised mice subjected to lethal IR (Fig. 1I).

In addition to acute hematopoietic syndrome, radiation can induce chronic BM injury principally due to HSC senescence, which may last a lifetime [29, 30]. Although conventional parameters largely recovered in mice 2 months after 5.0 Gy IR, HSC function was still abnormal at this time, which was characterized by elevated senescence-associated β-galactosidase (SA-β-gal) activity, myeloid skewing and loss of self-renewal ability [30–32]. Importantly, we discovered that exercise reduced SA-β-gal activity in HSCs 2 months after IR

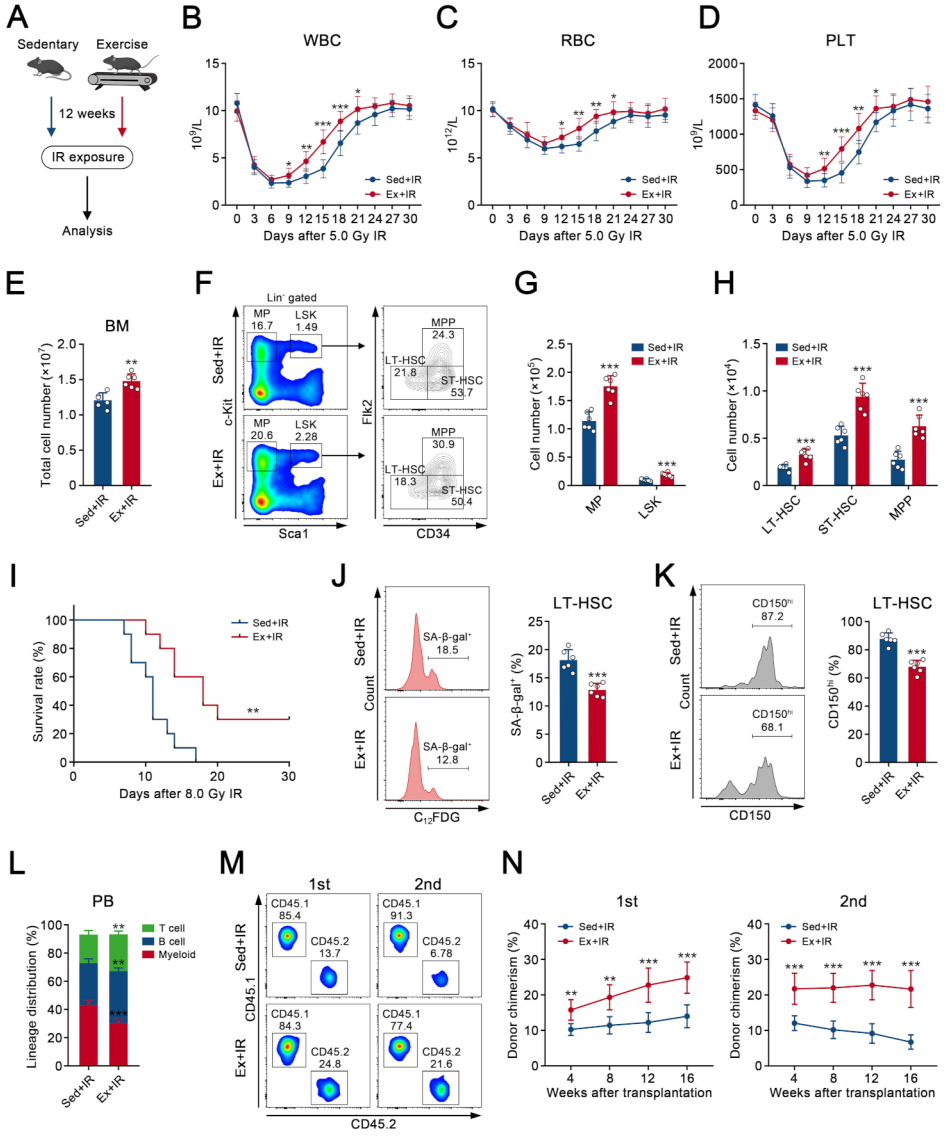

Fig. 1 Long-term moderate exercise alleviates IR-induced hematopoietic injury in mice. **(A)** The strategy of sedentary (Sed) or exercise (Ex) treatment in mice. (**B**-**D**) The counts of **(B)** WBCs, **(C)** RBCs and **(D)** PLTs in the PB of Sed or Ex mice at the indicated time after 5.0 Gy IR ($n = 10$). **(E)** The number of total BM cells (one femur and tibia) from Sed or Ex mice at day 15 after 5.0 Gy IR ($n = 10$). **(F)** Representative flow cytometric analysis of MPs, LSKs, LT-HSCs, ST-HSCs and MPPs from the BM of Sed or Ex mice at day 15 after 5.0 Gy IR. (**G**, **H**) The numbers of **(G)** MPs, LSKs, **(H)** LT-HSCs, ST-HSCs and MPPs in the BM (one femur and tibia) of Sed or Ex mice at day 15 after 5.0 Gy IR ($n = 6$). **(I)** The survival rates of Sed or Ex mice after 8.0 Gy IR ($n = 10$). **(J)** Flow cytometric analysis of the percentage of SA-β-gal$^+$ cells in LT-HSCs from the BM of Sed or Ex mice 2 months after 5.0 Gy IR ($n = 6$). **(K)** Flow cytometric analysis of the percentage of CD150^{hi} cells in LT-HSCs from the BM of Sed or Ex mice 2 months after 5.0 Gy IR ($n = 6$). **(L)** Flow cytometric analysis of the lineage distribution in the PB from Sed or Ex mice 2 months after 5.0 Gy IR ($n = 6$). (**M**, **N**) LT-HSCs isolated from the BM of Sed or Ex mice 2 months after 5.0 Gy IR, along with CD45.1 BM cells, were transplanted into lethally irradiated CD45.1 mice. Sixteen weeks later, the BM cells from primary recipients were transplanted into lethally irradiated secondary recipients. The percentage of CD45.2$^+$ cells in the PB of recipients at the indicated time after primary and secondary transplantation was analyzed by flow cytometry ($n = 6$). **(M)** Representative flow cytometric plots at 16 weeks after primary and secondary transplantation are shown. Data are shown as the mean ± SD. $^*P < 0.05$, $^{**}P < 0.01$, $^{***}P < 0.001$

(Fig. 1J). In addition, HSCs from exercised mice exhibited decreased myeloid skewing following IR exposure, as determined through the detection of the percentage of CD150^{hi} cells in LT-HSCs and the lineage distribution in the PB (Fig. 1K, L). To evaluate whether exercise could improve the self-renewal capacity of irradiated HSCs, we performed a competitive transplantation experiment using purified LT-HSCs (Supplementary Figure S1M). The chimerism levels of exercised mouse-derived cells in recipient mice were significantly greater than those in control-derived cells (Fig. 1M, N). Moreover, reduced myeloid reconstruction of irradiated HSCs was also

observed in exercised mice (Supplementary Figure S1N). Taken together, these findings suggested that exercise might play a critical role in counteracting acute and long-term BM injury following IR stress.

Exercise-generated carnosine contributes to protection against IR-induced HSC injury

Exercise can cause significant changes in multiple factors in the circulation that are secreted from skeletal muscles [24]. Carnosine is an endogenous dipeptide composed of β-alanine and L-histidine, the synthesis of which is catalyzed by carnosine synthase Carns1, which is mainly distributed in skeletal muscles [33, 34]. Studies have shown that carnosine is capable of accelerating the healing of IR-induced lung and testicular seminiferous tubule damage [35, 36]. Notably, carnosine levels gradually increased in the serum and BM ECF of mice after exercise (Fig. 2A; Supplementary Figures S2A-D), which was consistent with the findings of previous studies [37, 38]. To investigate whether carnosine mediated the radioprotective effect of exercise, we next generated a skeletal muscle-specific Carns1 knockout mouse model (Supplementary Figure S2E). Deletion of Carns1 was confirmed in the skeletal muscles of Carns1$^{flox/flox}$/HSA-Cre^{+} (hereafter referred to as Carn^{cKO}) mice but not Carns1$^{flox/flox}$/HSA-Cre^{-} (hereafter referred to as Carn$^{fl/fl}$) mice (Supplementary Figure S2F). Accordingly, even after exercise, carnosine was nearly undetectable in the BM ECF of Carn^{cKO} mice (Fig. 2B). Importantly, Carns1 deficiency largely abolished the protective effects of exercise on HSC injury caused by IR, although it was dispensable for homeostatic hematopoiesis (Fig. 2C-K; Supplementary Figures S2G-M). Hence, these findings illustrated that exercise protected HSCs from IR injury primarily by increasing carnosine production.

Carnosine injection ameliorates HSC damage in mice following IR exposure

To determine whether carnosine could serve as a potential radioprotective agent for hematopoiesis, we treated mice with different doses of carnosine in the context of IR (Fig. 3A). Compared with exercise, injecting doses greater than 50 mg/kg could achieve higher levels of carnosine in mice (Supplementary Figures S3A, B). It was found that carnosine increased the survival rate of mice, as well as acute hematopoietic recovery, after IR in a dose-dependent manner within 100 mg/kg, while the effects could be not further improved when the dose was increased to 200 mg/kg (Fig. 3B-F). On the basis of the above results, 100 mg/kg may be an ideal dose for further study, which may have a stronger antiradiation effect than exercise. Notably, flow cytometric analysis revealed that carnosine supplementation significantly increased the numbers of HSCs and various hematopoietic progenitor cells in the BM of irradiated mice (Fig. 3G-I; Supplementary Figure S3C). Similarly, IR-induced HSC senescence was also substantially mitigated in mice when treated with carnosine (Fig. 3J-M; Supplementary Figures S3D, E). These data indicated that carnosine could effectively ameliorate BM damage caused by IR.

Carnosine protects HSCs from IR via the transporter Slc15a2

Current studies suggest that carnosine crosses the cellular membrane primarily via the oligopeptide transporter family members Slc15a1-4 [39, 40]. Through analysis of public microarray data and our previously published RNA-seq data, we found that Slc15a2 was highly expressed in HSCs from the BM of normal mice (Fig. 4A, B). This finding was further verified by qPCR analysis of purified BM subpopulations (Fig. 4C). To clarify whether Slc15a2 mediated the radioprotective effect of carnosine, we used hematopoietic-specific Slc15a2 conditional knockout mice (Supplementary Figure S4A). Compared with Slc15a2$^{flox/flox}$/Mx1-Cre^{-} (hereafter, referred to as Slc$^{fl/fl}$) mice, Slc15a2 depletion was only induced in hematopoietic cells from Slc15a2$^{flox/flox}$/Mx1-Cre^{+} (hereafter, referred to as Slc^{cKO}) mice by pIpC injection (Supplementary Figure S4B). However, we discovered that Slc15a2 was not essential for adult hematopoiesis at steady state (Supplementary Figures S4C-G). Intriguingly, carnosine injection accelerated acute hematopoietic recovery and increased the survival rate in normal mice but not in Slc15a2-deficient mice following IR (Fig. 4D-H). Moreover, carnosine supplementation did not inhibit IR-induced long-term functional compromise in HSCs after Slc15a2 ablation (Fig. 4I-L). Overall, the uptake of carnosine by Slc15a2 was required to facilitate hematopoietic regeneration after IR.

Carnosine facilitates the proliferation and survival of HSCs after IR

To obtain insight into the underlying molecular mechanism, we subsequently performed an RNA-seq analysis. The data revealed that a total of 2550 genes were differentially expressed between the saline and carnosine-treated groups after IR, whereas only 503 DEGs were found in those without IR (Fig. 5A; Supplementary Figure S5A), suggesting that carnosine treatment mainly changed the transcriptional levels in HSCs under IR conditions. Interestingly, GSEA revealed that cell cycle- and proliferation-associated genes were upregulated, whereas quiescence-associated genes were downregulated in irradiated HSCs treated with carnosine (Fig. 5B). Consistent with these findings, cell cycle analysis revealed that the percentage of HSCs in the G0 phase was decreased and that the percentage of HSCs in the G1 and S/G2/M phases was increased following carnosine administration,

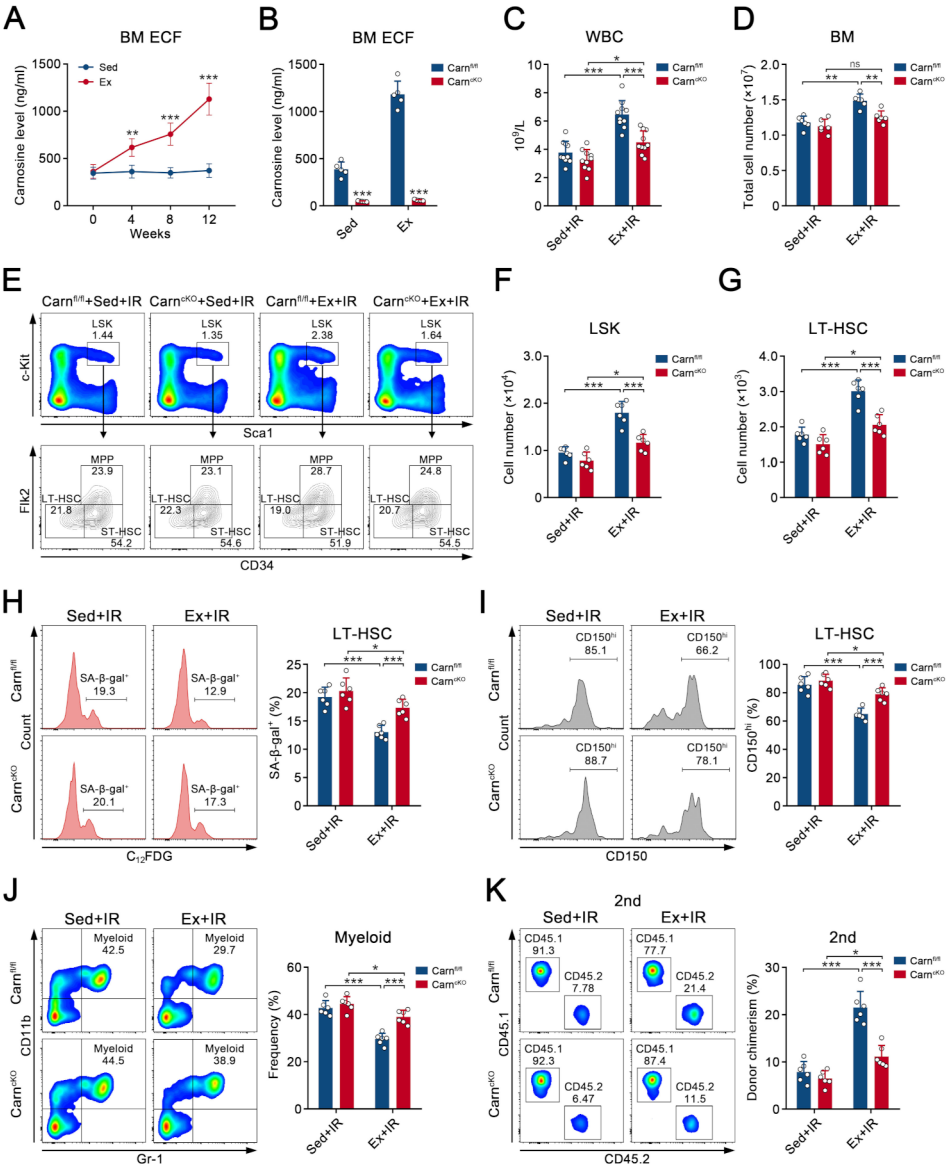

Fig. 2 Exercise-generated carnosine contributes to protecting HSC injury from IR. **(A)** The levels of carnosine in the BM ECF of mice at the indicated time after Sed and Ex treatment ($n=5$). **(B)** The levels of carnosine in the BM ECF of Carn$^{fl/fl}$ or Carn^{cKO} mice with or without exercise for 12 weeks ($n=5$). A twelve weeks exercise program was used for subsequent experiments. **(C)** The counts of WBCs in the PB of Carn$^{fl/fl}$ or Carn^{cKO} mice with or without exercise at day 15 after 5.0 Gy IR ($n=10$). **(D)** The number of total BM cells (one femur and tibia) from Carn$^{fl/fl}$ or Carn^{cKO} mice with or without exercise at day 15 after 5.0 Gy IR ($n=6$). **(E)** Representative flow cytometric analysis of LSKs and LT-HSCs from the BM of Carn$^{fl/fl}$ or Carn^{cKO} mice with or without exercise at day 15 after 5.0 Gy IR. (**F**, **G**) The number of **(F)** LSKs and **(G)** LT-HSCs in the BM (one femur and tibia) of Carn$^{fl/fl}$ or Carn^{cKO} mice with or without exercise at day 15 after 5.0 Gy IR ($n=6$). **(H)** Flow cytometric analysis of the percentage of SA-β-gal$^+$ cells in LT-HSCs from the BM of Carn$^{fl/fl}$ or Carn^{cKO} mice with or without exercise 2 months after 5.0 Gy IR ($n=6$). **(I)** Flow cytometric analysis of the percentage of CD150^{hi} cells in LT-HSCs from the BM of Carn$^{fl/fl}$ or Carn^{cKO} mice with or without exercise 2 months after 5.0 Gy IR ($n=6$). **(J)** Flow cytometric analysis of the lineage distribution in the PB from Carn$^{fl/fl}$ or Carn^{cKO} mice with or without exercise 2 months after 5.0 Gy IR ($n=6$). **(K)** LT-HSCs isolated from the BM of Carn$^{fl/fl}$ or Carn^{cKO} mice with or without exercise 2 months after 5.0 Gy IR, along with CD45.1 BM cells, were transplanted into lethally irradiated CD45.1 mice. Sixteen weeks later, the BM cells from primary recipients were transplanted into lethally irradiated secondary recipients. The percentage of CD45.2$^+$ cells in the PB of recipients at 16 weeks after secondary transplantation was analyzed by flow cytometry ($n=6$). Data are shown as the mean ± SD. ns, not significant. $^*P<0.05$, $^{**}P<0.01$, $^{***}P<0.001$

which was further corroborated by the in vivo BrdU incorporation assay (Fig. 5 C, D). As anticipated, HSCs from IR-exposed mice injected with carnosine presented increased colony formation in vitro (Fig. 5E). On the other hand, GSEA revealed that carnosine supplementation inhibited IR-induced apoptosis in HSCs, which was verified by flow cytometric analysis (Fig. 5B, F). Similar results were obtained from the in vitro assay, with 40

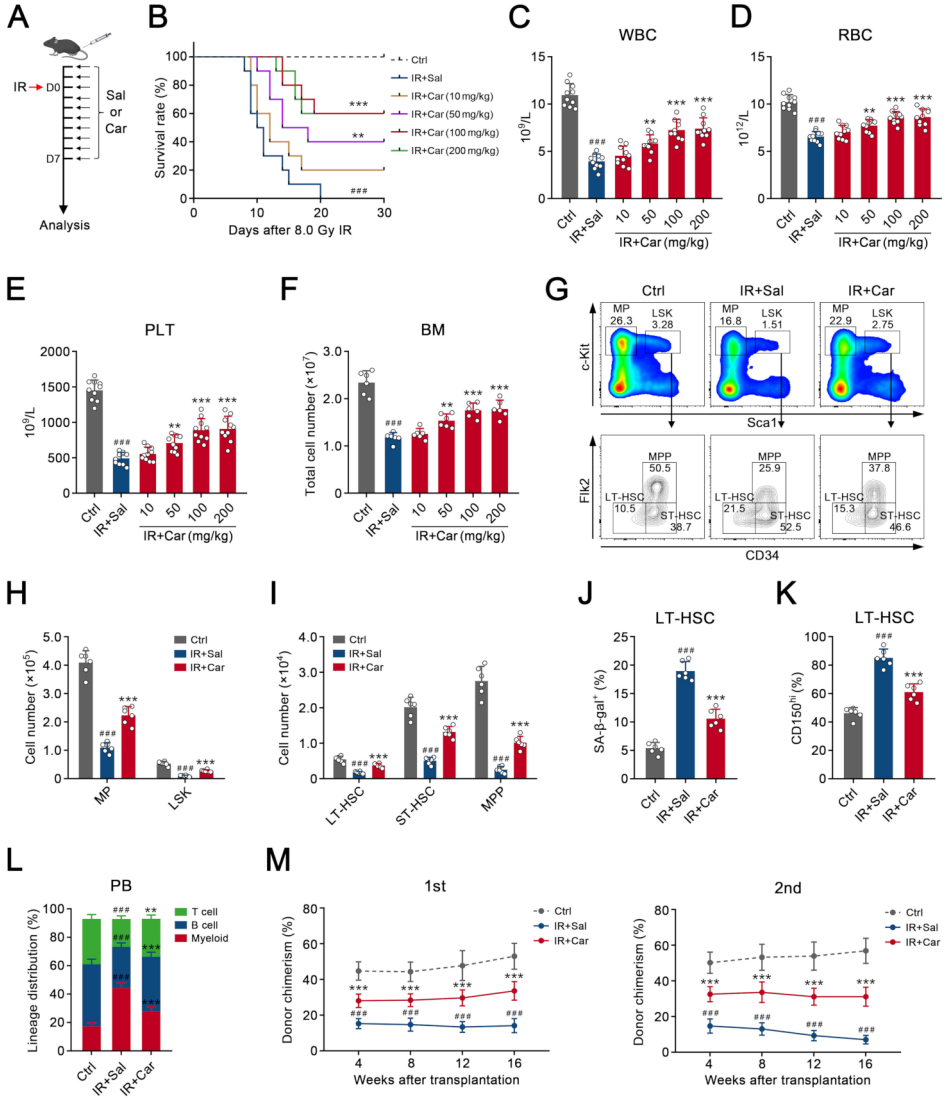

Fig. 3 Carnosine injection ameliorates the damage of HSCs in mice following IR exposure. **(A)** The strategy of IR and saline (Sal) or carnosine (Car) injection in mice. **(B)** The survival rate of control (Ctrl) mice or mice treated with Sal or different doses of Car (10, 50, 100 or 200 mg/kg) after 8.0 Gy lethally IR ($n=10$). (**C**-**E**) The counts of **(C)** WBCs, **(D)** RBCs and **(E)** PLTs in the PB of Ctrl mice or mice treated with Sal or different doses of Car at day 15 after 5.0 Gy IR ($n=10$). **(F)** The number of total BM cells (one femur and tibia) from Ctrl mice or mice treated with Sal or different doses of Car at day 15 after 5.0 Gy IR ($n=6$). A 100 mg/kg injection dose of Car was used for subsequent experiments. **(G)** Representative flow cytometric analysis of MPs, LSKs, LT-HSCs, ST-HSCs and MPPs from the BM of Ctrl mice or mice treated with Sal or Car at day 15 after 5.0 Gy IR. (**H**, **I**) The numbers of **(H)** MPs, LSKs, **(I)** LT-HSCs, ST-HSCs and MPPs in the BM (one femur and tibia) of Ctrl mice or mice treated with Sal or Car at day 15 after 5.0 Gy IR ($n=6$). **(J)** Flow cytometric analysis of the percentage of SA-β-gal$^+$ cells in LT-HSCs from the BM of Ctrl mice or mice treated with Sal or Car 2 months after 5.0 Gy IR ($n=6$). **(K)** Flow cytometric analysis of the percentage of CD150^{hi} cells in LT-HSCs from the BM of Ctrl mice or mice treated with Sal or Car 2 months after 5.0 Gy IR ($n=6$). **(L)** Flow cytometric analysis of the lineage distribution in the PB from Ctrl mice or mice treated with Sal or Car 2 months after 5.0 Gy IR ($n=6$). **(M)** LT-HSCs isolated from the BM of Ctrl mice or mice treated with Sal or Car 2 months after 5.0 Gy IR, along with CD45.1 BM cells, were transplanted into lethally irradiated CD45.1 mice. Sixteen weeks later, the BM cells from primary recipients were transplanted into lethally irradiated secondary recipients. The percentage of CD45.2$^+$ cells in the PB of recipients at the indicated time after primary and secondary transplantation was analyzed by flow cytometry ($n=6$). Data are shown as the mean ± SD. Compared with IR + Sal group, $^{**}P<0.01$, $^{***}P<0.001$; Compared with Ctrl group, $^{\#\#\#}P<0.001$

μM as the optimal carnosine concentration (Supplementary Figure S5B). Furthermore, through analysis of genes related to the cell cycle based on the RNA-seq data, we observed that expression of the cyclin-dependent kinase inhibitor p21 was markedly reduced in irradiated HSCs treated with carnosine (Fig. 5A). In addition, carnosine strikingly attenuated the expression of Puma, a dominant gene that drives HSC apoptosis [41], after IR (Fig. 5A). These results were further confirmed at the mRNA and protein levels (Fig. 5G-J, Supplementary Figures S5C,

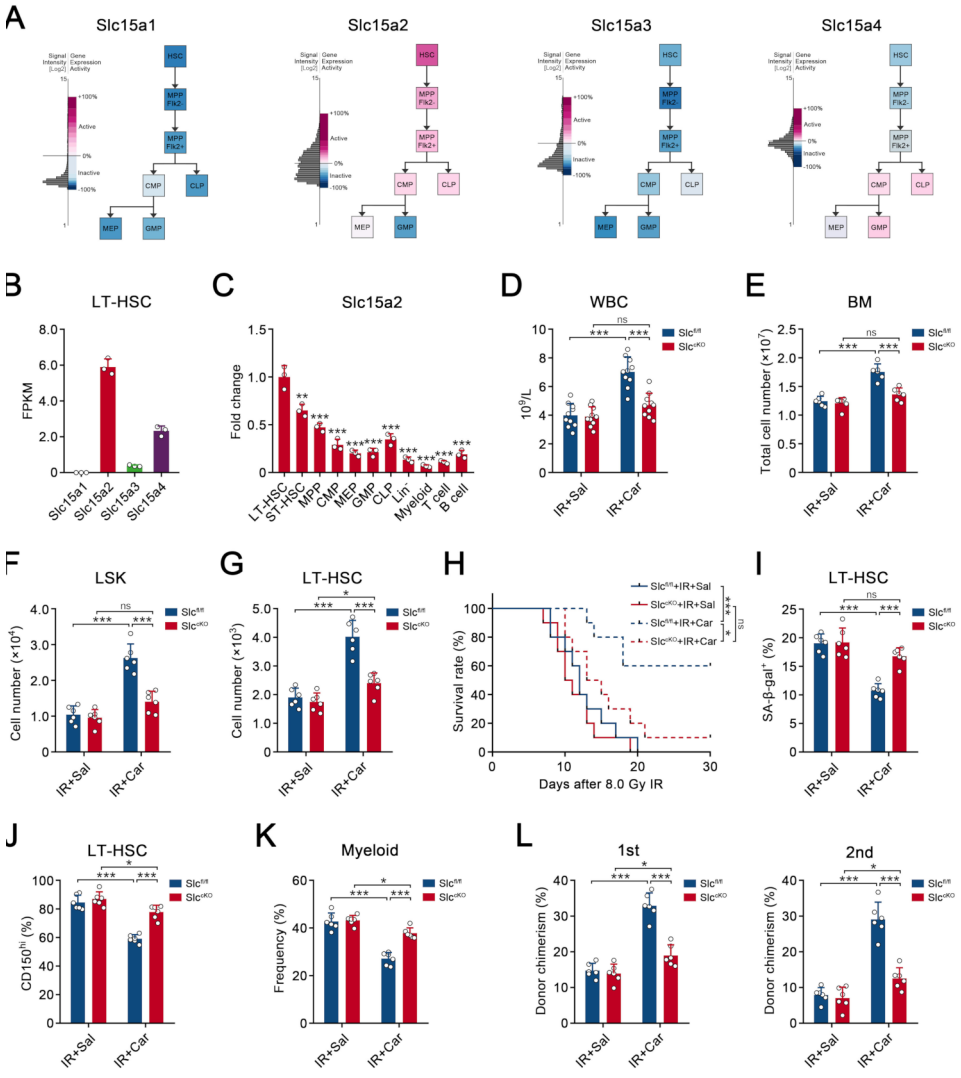

Fig. 4 Carnosine protects HSCs from IR via the transporter Slc15a2. **(A)** The expression of Slc15a1-4 in murine hematopoietic cells. Data were obtained from the Gene Expression Commons database. **(B)** The expression of Slc15a1-4 in LT-HSCs from the BM of normal mice ($n=3$). Data were obtained from SRA database (No. PRJNA891790). **(C)** qPCR analysis of expression of Slc15a2 in the indicated cell populations purified from the BM of normal mice ($n=3$). The relative expression of Slc15a2 was compared with that in LT-HSCs. **(D)** The counts of WBCs in the PB of $Slc^{fl/fl}$ or Slc^{cKO} mice treated with Sal or Car at day 15 after 5.0 Gy IR ($n=10$). **(E)** The number of total BM cells (one femur and tibia) from $Slc^{fl/fl}$ or Slc^{cKO} mice treated with Sal or Car at day 15 after 5.0 Gy IR ($n=6$). (**F**, **G**) The numbers of **(F)** LSKs and **(G)** LT-HSCs in the BM (one femur and tibia) of $Slc^{fl/fl}$ or Slc^{cKO} mice treated with Sal or Car at day 15 after 5.0 Gy IR ($n=6$). (H) The survival rates of $Slc^{fl/fl}$ or Slc^{cKO} mice treated with Sal or Car after 8.0 lethally Gy IR ($n=10$). **(I)** Flow cytometric analysis of the percentage of SA-β-gal$^+$ cells in LT-HSCs from the BM of $Slc^{fl/fl}$ or Slc^{cKO} mice treated with Sal or Car 2 months after 5.0 Gy IR ($n=6$). **(J)** Flow cytometric analysis of the percentage of CD150^{hi} cells in LT-HSCs from the BM of $Slc^{fl/fl}$ or Slc^{cKO} mice treated with Sal or Car 2 months after 5.0 Gy IR ($n=6$). **(K)** Flow cytometric analysis of the percentage of myeloid cells in PB of $Slc^{fl/fl}$ or Slc^{cKO} mice treated with Sal or Car 2 months after 5.0 Gy IR ($n=6$). **(L)** LT-HSCs isolated from the BM of $Slc^{fl/fl}$ or Slc^{cKO} mice treated with Sal or Car 2 months after 5.0 Gy IR, along with CD45.1 BM cells, were transplanted into lethally irradiated CD45.1 mice. Sixteen weeks later, the BM cells from primary recipients were transplanted into lethally irradiated secondary recipients. The percentage of CD45.2$^+$ cells in the PB of recipients at 16 weeks after primary and secondary transplantation was analyzed by Flow cytometry ($n=6$). Data are shown as the mean ± SD. ns, not significant. *$P<0.05$, **$P<0.01$, ***$P<0.001$

D). In contrast, other cell cycle- or apoptosis-associated genes, with the exception of p27, which was slightly downregulated, were largely unchanged (Supplementary Figures S5C, D). Importantly, the above effects of carnosine were largely abrogated in the absence of Slc15a2 (Supplementary Figures S5E-H). Of note, exercise had a similar role in facilitating HSC expansion and survival after IR, which disappeared after the deletion of Carns1 in skeletal muscle (Supplementary Figures S5I-L). Thus, carnosine accelerated hematopoietic recovery post-IR, likely by regulating the proliferation and apoptosis of HSCs.

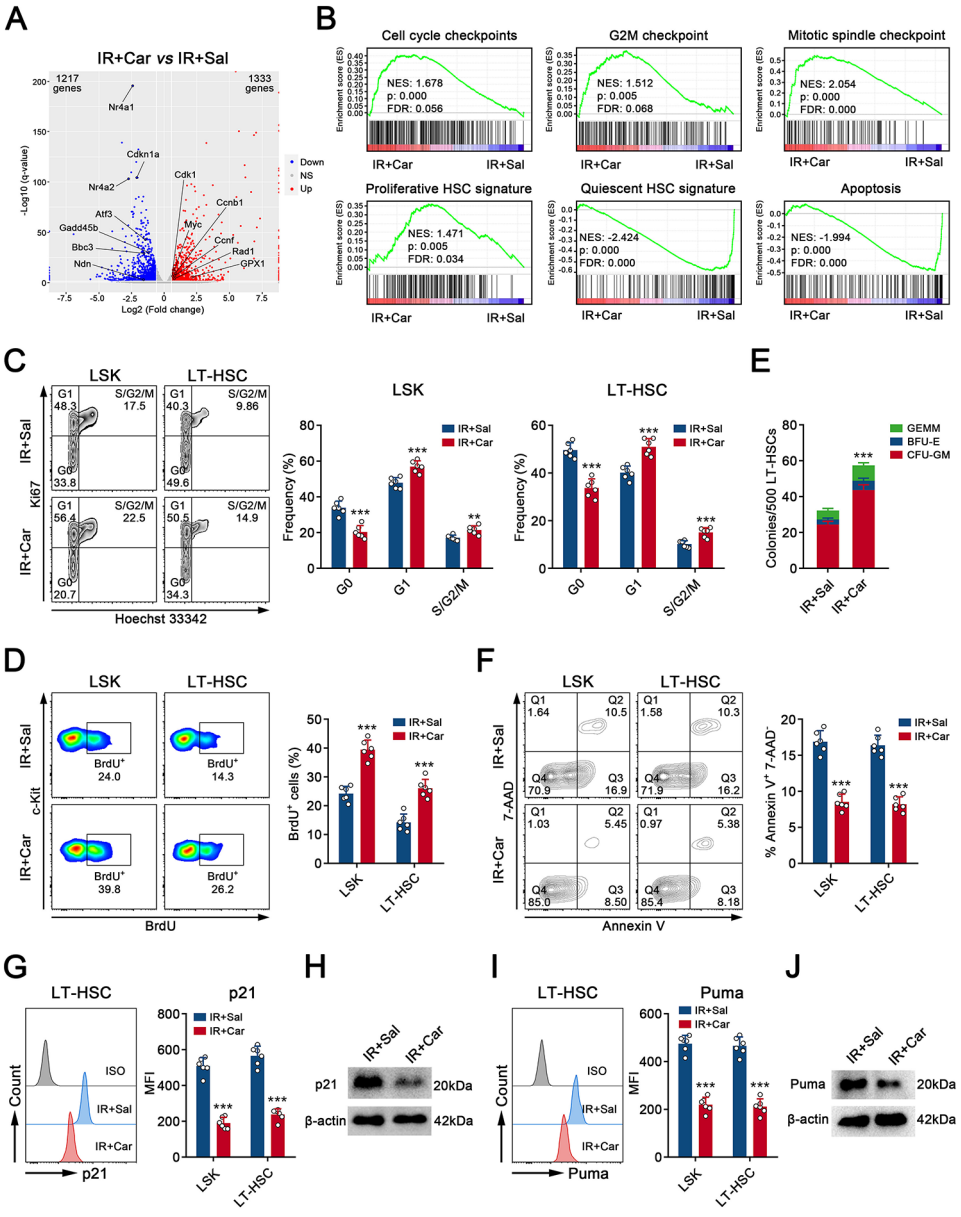

Fig. 5 Carnosine facilitates the proliferation and survival of HSCs post IR. (**A**, **B**) RNA-Seq analysis of LT-HSCs in the BM of mice treated with Sal or Car at day 15 after 5.0 Gy IR ($n=3$). **(A)** Volcano plot revealing the DEGs between two groups. **(B)** GSEA of the indicated gene sets using the RNA-Seq data. **(C)** Flow cytometric analysis of the cell cycle of LSKs and LT-HSCs from the BM of mice treated with Sal or Car at day 15 after 5.0 Gy IR ($n=6$). **(D)** Flow cytometric analysis of the in vivo BrdU incorporation in LSKs and LT-HSCs from the BM of mice treated with Sal or Car at day 15 after 5.0 Gy IR ($n=6$). **(E)** Colony formation analysis of LT-HSCs from the BM of mice treated with Sal or Car at day 15 after 5.0 Gy IR ($n=5$). **(F)** Flow cytometric analysis of the apoptosis of LSKs and LT-HSCs from the BM of mice treated with Sal or Car at day 15 after 5.0 Gy IR ($n=6$). **(G)** Flow cytometric analysis of the expression of p21 in LSKs and LT-HSCs from the BM of mice treated with Sal or Car at day 15 after 5.0 Gy IR ($n=6$). **(H)** Western blot analysis of the expression of p21 in LSKs sorted from the BM of mice treated with Sal or Car at day 15 after 5.0 Gy IR ($n=7$–8 mice were pooled). **(I)** Flow cytometric analysis of the expression of Puma in LSKs and LT-HSCs from the BM of mice treated with Sal or Car at day 15 after 5.0 Gy IR ($n=6$). **(J)** Western blot analysis of the expression of Puma in LSKs sorted from the BM of mice treated with Sal or Car at day 15 after 5.0 Gy IR ($n=7$–8 mice were pooled). Data are shown as the mean ± SD. $^{**}P<0.01$, $^{***}P<0.001$

Carnosine directly inhibits the transcriptional activity of p53 in HSCs after IR

Increased p53 activity after IR is accountable for cell cycle arrest and apoptosis in HSCs, which results in acute hematopoietic injury [42, 43]. In addition, hyperactivation of the p53/p21 axis can irreversibly arrest the cell cycle, ultimately inducing HSC senescence and residual myelosuppression following IR exposure [9, 44]. Notably, the p53 signaling pathway and p53 targets markedly dampened in irradiated HSCs after carnosine intervention (Fig. 6A). Indeed, the effector molecules p21 and Puma are direct targets of p53 and can initiate

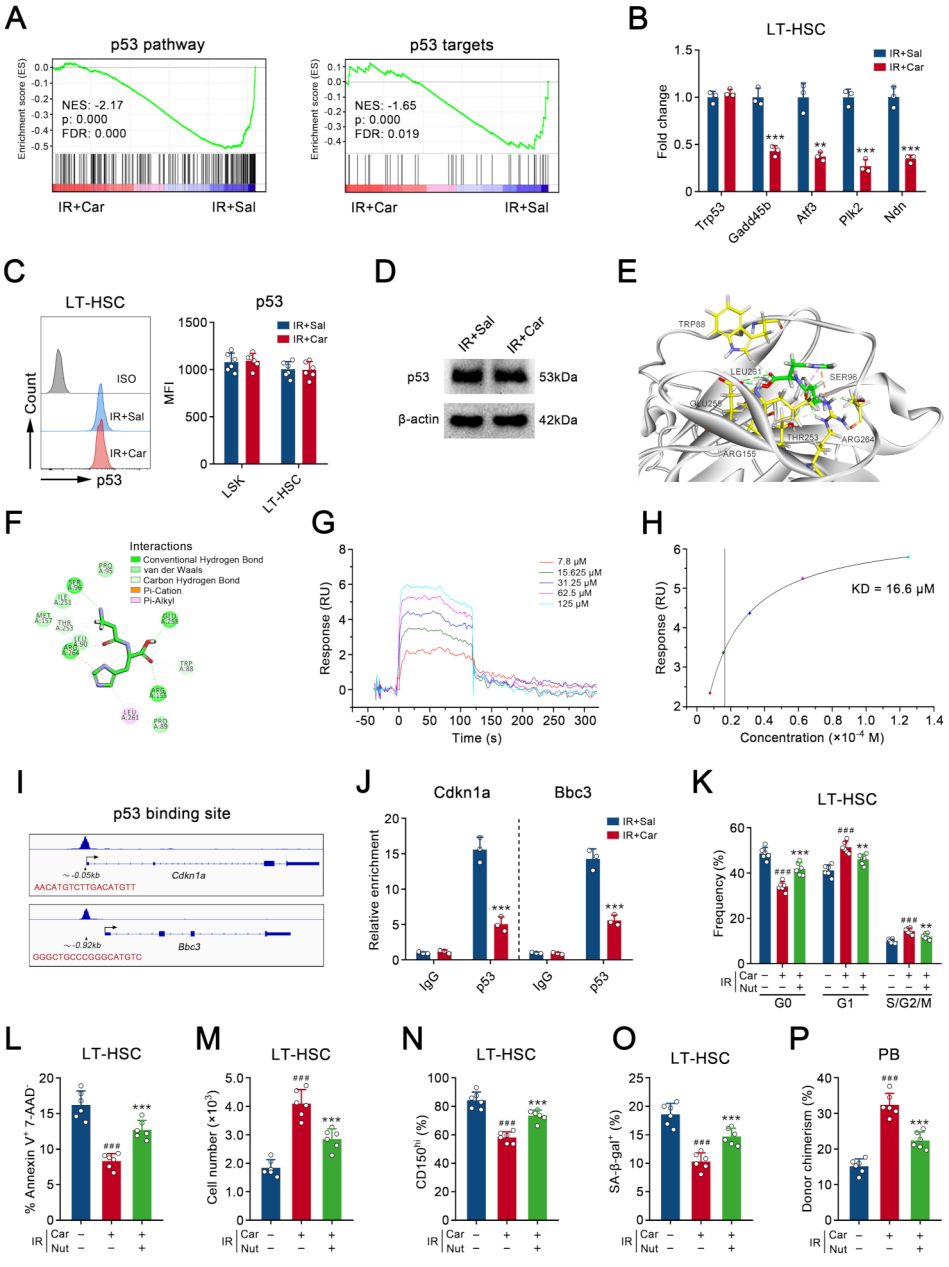

Fig. 6 Carnosine directly inhibits the transcriptional activity of p53 in HSCs after IR. **(A)** GSEA of the p53 pathway and p53 targets using the RNA-Seq data obtained from LT-HSCs in the BM of mice treated with Sal or Car at day 15 after 5.0 Gy IR. **(B)** qPCR analysis of the expression of p53 and its target genes in LT-HSCs sorted from the BM of mice treated with Sal or Car at day 15 after 5.0 Gy IR ($n=3$). **(C)** Flow cytometric analysis of the expression of p53 in LSKs and LT-HSCs from the BM of mice treated with Sal or Car at day 15 after 5.0 Gy IR ($n=6$). **(D)** Western blot analysis of the expression of p53 in LSKs sorted from the BM of mice treated with Sal or Car at day 15 after 5.0 Gy IR ($n=7$–8 mice were pooled). (**E**, **F**) Molecular docking shows the interaction of carnosine with p53 and the binding energy is -8.56 kcal/mol. (**G**, **H**) SPR analysis of the binding affinity of carnosine with p53. **(I)** ChIP-seq analysis revealing the p53 binding sites in the promoter region of Cdkn1a and Bbc3 gene in mice. Data were obtained from BioStudies database (No. E-MTAB-3954). **(J)** ChIP analysis of the binding of p53 to the promoter region of Cdkn1a and Bbc3 in LSKs from the BM of mice treated with Sal or Car at day 15 after 5.0 Gy IR ($n=3$). Cdkn1a, the gene name of p21; Bbc3, the gene name of Puma. **(K)** Flow cytometric analysis of the cell cycle of LT-HSCs from the BM of mice treated with Sal or Car, along with Veh or Nutlin-3a (Nut), at day 15 after 5.0 Gy IR ($n=6$). **(L)** Flow cytometric analysis of the apoptosis of LT-HSCs from the BM of mice treated with Sal or Car, along with Veh or Nut, at day 15 after 5.0 Gy IR ($n=6$). **(M)** The number of LT-HSCs in the BM (one femur and tibia) of mice treated with Sal or Car, along with Veh or Nut, at day 15 after 5.0 Gy IR ($n=6$). **(N)** Flow cytometric analysis of the percentage of $CD150^{hi}$ cells in LT-HSCs from the BM of mice treated with Sal or Car, along with Veh or Nut, 2 months after 5.0 Gy IR ($n=6$). **(O)** Flow cytometric analysis of the percentage of SA-β-gal^+ cells in LT-HSCs from the BM of mice treated with Sal or Car, along with Veh or Nut, 2 months after 5.0 Gy IR ($n=6$). **(P)** LT-HSCs isolated from the BM of mice treated with Sal or Car, along with Veh or Nut, 2 months after 5.0 Gy IR were transplanted into lethally irradiated CD45.1 mice, together with CD45.1 BM cells. The percentage of $CD45.2^+$ cells in the PB of recipients at 16 weeks after transplantation was analyzed by flow cytometry ($n=6$). Compared with IR + Sal or IR + Car + Veh group, $^{**}P<0.01$, $^{***}P<0.001$; Compared with IR + Sal + Veh group, $^{###}P<0.001$

transcription after binding to specific DNA regions [44]. In addition, decreases in other p53 downstream genes were verified in irradiated HSCs in the presence of carnosine (Fig. 6B). Surprisingly, carnosine treatment did not affect the expression of p53 itself or p-p53, in HSCs following IR (Fig. 6B-D; Supplementary Figures S6A, B). These data prompted us to speculate that carnosine might be involved in directly suppressing the transcriptional activity of p53. To validate this notion, we next conducted a molecular docking analysis of the p53 protein with carnosine and found that carnosine had a high affinity for p53 (Fig. 6E, F). Importantly, most amino acid residues that interact with carnosine were located in the core DNA-binding domain of p53 (residues 92–292), such as SSR96, ARG264, ARG155, and GLU255 (Fig. 6E, F). Subsequently, an SPR assay revealed that the equilibrium dissociation (KD value) was 16.6 μM for the interaction of p53 with carnosine (Fig. 6G, H). On the other hand, a ChIP assay revealed an evident decrease in p53-mediated transcriptional activation of Cdkn1a and Bbc3 in irradiated HSCs after carnosine administration, further reinforcing our findings (Fig. 6I, J).

To determine whether carnosine functions was dependent on p53, we used the p53 agonist Nutlin-3a, which can prevent p53 protein degradation by inhibiting the interaction of the E3-ubiquitin ligase Mdm2 with p53 [45, 46]. The upregulation of the expression of p53 was determined in HSCs after Nutlin-3a treatment (Supplementary Figure S6C). As expected, Nutlin-3a administration increased the levels of p21 and Puma in irradiated HSCs treated with carnosine, thereby partly abolishing the radioprotective effect of carnosine (Fig. 6K-P; Supplementary Figures S6D-J).

The carnosine/SLC15A2-p53 axis protects human HSCs from IR-induced injury

Finally, we sought to identify whether carnosine had a similar effect on human HSCs. The data from the public microarray database revealed that SLC15A2 is also highly enriched in human HSCs, which was verified by qPCR analysis (Fig. 7A; Supplementary Figures S7A, B). Subsequently, we knocked down SLC15A2 expression in human CB $CD34^+$ cells, and found that shSLC15A2-2 was a great shRNA to downregulate the expression of SLC15A2 (Fig. 7B; Supplementary Figure S7C). Consistent with the data from mice, knockdown of SLC15A2 did not obviously affect the phenotype and function of human HSCs without IR (Supplementary Figures S7D-F). Importantly, following IR exposure, the addition of carnosine impeded the decrease in total cell number and the percentage of HSCs in culture, whereas these changes almost disappeared after SLC15A2 knockdown (Fig. 7C, D). Moreover, carnosine treatment stimulated the proliferation and suppressed the apoptosis of irradiated HSCs in the presence of SLC15A2 (Fig. 7E, F). Consequently, compared with the shSLC15A2 (hereafter referred to as the shSLC) group, shCtrl HSCs treated with carnosine after IR exhibited a greater ability to repopulate hematopoiesis in M-NSG mice, together with reduced myeloid-skewed differentiation (Fig. 7G-I). Furthermore, the carnosine/SLC15A2 axis-mediated inactivation of the p53 signaling pathway in HSCs following IR was determined by detecting the expression of p21 and Puma at both the mRNA and protein levels (Fig. 7J; Supplementary Figures S7G-I). In summary, our data revealed that carnosine played an important role in mitigating IR-induced HSC injury by inhibiting p53 activation (Fig. 7K).

Discussion

The hematopoietic system is extraordinarily vulnerable to radiation injury, resulting in life-threatening changes including anemia, bleeding and infection [5, 8]. The depletion of functional HSCs, which can self-renew and differentiate into all types of blood cells, commonly occurs in people receiving intentional or accidental radiation exposure [47, 48]. After decades of research, the intrinsic mechanism of radiation damage specific to hematopoietic tissue has gradually been elucidated. However, the availability of suitable measures to protect against radiation is relatively insufficient. In the present study, we revealed for the first time that exercise-generated carnosine could alleviate acute and long-term hematopoietic injury after IR by restricting activation of the p53 signaling pathway in HSCs.

It is known that physical exercise has a profound impact on multiple tissues or organs in different ways [13, 24]. In this study, we systematically evaluated the effect of long-term moderate exercise on hematopoiesis in the context of IR and reported that exercise significantly mitigated IR-induced acute myelosuppression in mice, which is strongly supported by related studies [14, 20–22]. Meantime, our data revealed that IR-induced residual BM injury resulting from HSC senescence was also alleviated by exercise. Previous studies have focused more on classic factors generated from skeletal muscles, whereas carnosine, a multifunctional histidine-containing dipeptide, has been largely overlooked [24, 49]. On the basis of its biological characteristics, carnosine is involved in a variety of biological processes [34]. Notably, recent studies have reported that carnosine can relieve the BM damage induced by cyclophosphamide [50, 51]. Intriguingly, specific deletion of Carns1 in skeletal muscles largely abrogated the exercise-mediated effects on HSCs after radiation, although exercise retained some effects on irradiated HSCs in $Carn^{cKO}$ mice. These observations may be due to some other factors, such as IL-6, IGF-1 and FGF-2, also secreted by the muscles after exercise [24]. Specifically, we found that the carnosine

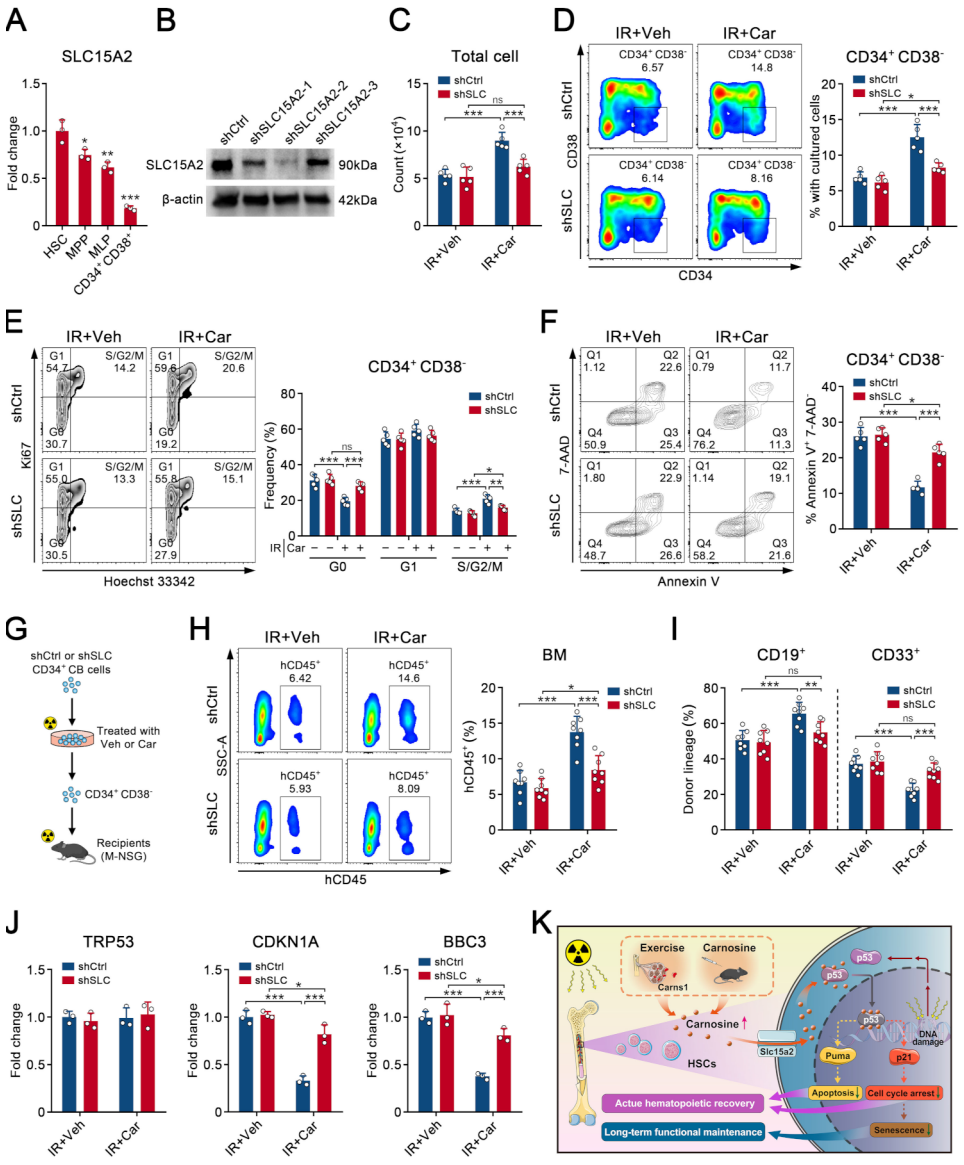

Fig. 7 Carnosine/SLC15A2-p53 axis prevents human HSCs from IR-induced injury. **(A)** qPCR analysis of expression of SLC15A2 in the indicated cell populations purified from human CB ($n=3$). The relative expression SLC15A2 was compared with that in HSCs. (B) Western blot analysis of expression of SLC15A2 in CB CD34$^+$ cells after transfected with lentivirus carrying shCtrl, shSLC15A2-1, shSLC15A2-2 or shSLC15A2-3 ($n=3$). (**C**-**I**) Human CB CD34$^+$ cells transfected with shCtrl or shSLC were subjected to 2.0 Gy IR in the presence of Veh or Car. These cells were cultured for 10 days and then used for further analysis. **(C)** The number of total cells in the culture ($n=5$). **(D)** Flow cytometric analysis of the percentage of CD34$^+$ CD38$^-$ cells in the culture ($n=5$). **(E)** Flow cytometric analysis of the cell cycle of CD34$^+$ CD38$^-$ cells in the culture ($n=5$). **(F)** Flow cytometric analysis of the apoptosis of CD34$^+$ CD38$^-$ cells in the culture ($n=5$). (**G**-**I**) CD34$^+$ CD38$^-$ cells isolated from the cultured cells were transplanted into irradiated M-NSG mice. **(G)** The strategy of xenotransplantation. **(H)** The percentage of hCD45$^+$ cells in the BM of recipients at 16 weeks after transplantation ($n=8$). **(I)** The lineage distribution of hCD45$^+$ cells in the BM of recipients at 16 weeks after transplantation ($n=8$). **(J)** qPCR analysis of expression of TRP53, CDKN1A and BBC3 in CD34$^+$ CD38$^-$ cells purified from cultured cells ($n=3$). **(K)** The schematic diagram showing how carnosine alleviates IR-induced hematopoietic injury. Data are shown as the mean ± SD. ns, not significant. *$P<0.05$, **$P<0.01$, ***$P<0.001$

transporter Slc15a2 was highly expressed in mouse and human HSCs. Similar to that in exercised mice, acute hematopoietic recovery was substantially increased in irradiated mice after carnosine injection. Similarly, HSC senescence was evidently reversed in irradiated mice treated with carnosine, which is in accordance with the findings that both exercise and carnosine supplementation have the ability to treat aging-related diseases, such as Alzheimer's disease, Parkinson's disease and atherosclerosis [52–56]. However, carnosine showed a slight radioprotective effect on Slc15a2-deficient HSCs, indicating that another transporter Slc15a4 might still allow

partial carnosine's transport in HSCs. Alternatively, carnosine may regulate HSCs via an extrinsic mechanism, such as in a microenvironment-dependent manner. Collectively, these data indicated that exercise or carnosine supplementation could be a potential strategy to increase resistance of the body to IR.

Previous studies, including our own work, have indicated that HSCs are maintained in a quiescent state to preserve their self-renewal ability [3, 26]. However, excessive suppression of HSC activation may dampen hematopoietic reconstitution during acute BM injury [6, 47]. In addition, irreversible cell cycle arrest may cause HSC senescence, leading to long-term hematopoietic suppression [44]. In this work, exercise or the addition of carnosine promoted the rapid proliferation of HSCs after IR. On the other hand, the extreme increase in apoptosis, a fundamental reason for the decrease in the number of HSCs after IR, was distinctly alleviated by exercise or carnosine intervention. Accumulating evidence reveals that overactivation of p53 contributes to cell cycle inhibition and apoptosis after IR, whereas alternative p53 inhibitors, especially those used in hematopoiesis, are relatively rare [43, 46]. Interestingly, the p53 signaling pathway was significantly decreased in IR-exposed HSCs after carnosine treatment. On the basis of RNA-seq analysis, we discovered that expression of the cell cycle inhibitor p21 and the proapoptotic factor Puma, which are downstream target genes of p53, was significantly downregulated in irradiated HSCs after carnosine administration. Taken together, these findings indicated that skeletal muscle-derived carnosine promoted the proliferation and survival of HSCs subjected to IR injury.

DNA double-strand breaks caused by IR can be recognized by ataxia telangiectasia mutated (ATM), which subsequently activates p53 via direct and indirect phosphorylation [9]. However, the level of p53 phosphorylation was comparable between irradiated HSCs treated with or without carnosine. As a small molecule, carnosine has been shown to bind certain target proteins, such as GNMT and MMP-9, thereby regulating their function [57, 58]. These findings suggest that carnosine may be involved in directly inhibiting the activity of p53 independent of its phosphorylation. Molecular docking, combined with SPR assay, revealed that carnosine could interact with p53 protein, especially the DNA-binding domain. Furthermore, the transcriptional activity of p53 was markedly compromised in HSCs in the presence of carnosine, as determined by ChIP analysis. Consequently, increasing p53 protein levels via Nutlin-3a partially counteracted the effects of carnosine on HSCs after IR, further strengthening our hypothesis. Carnosine ameliorates IR-induced hematopoietic injury, at least in part, by regulating p53 activity. On the other hand, many antioxidants, such as metformin, nicotinamide riboside, and grape seed proanthocyanidin extract, possess better antiradiation effects [59–61]. Since carnosine has the ability to scavenge active oxygen species (ROS), we assume that this capability may also play a role. Moreover, data obtained from extensive cell and animal experiments have shown that carnosine has few side effects within a certain dose range [34, 40]. Hence, carnosine may be a promising and safe radiation protectant. Additionally, in order to avoid potential estrogen interference in irradiation, we used only male mice to carried out the study. The role of carnosine in female mice and whether carnosine has a coordinated effect with estrogen still need extra investigations.

In conclusion, our findings demonstrate that skeletal muscle-derived carnosine is an ideal agent for mitigating hematopoietic injury induced by IR through the inhibition of p53-dependent cell cycle arrest and apoptosis in HSCs. These data reveal a critical role of exercise or carnosine supplementation in facilitating HSC regeneration, providing therapeutic approaches for patients experiencing myeloablative stress.

Supplementary Information

The online version contains supplementary material available at https://doi.org/10.1186/s12964-024-01959-2.

Supplementary Material 1

Acknowledgements
We thank Prof. Jinyong Wang for gifting CD45.1 mice, and Yang Liu for technical support in flow cytometry.

Author contributions
H.Z. and N.C. designed the study, performed experiments, analyzed data and wrote the paper. F.C. and X.Z. performed experiments and analyzed data. L.Y. and Y.L. participated in some animal experiments. M.C., M.S. and S.W. participated in data analysis. S.C., J.C., X.Z., J.Z. and Y.X. participated in the initial experimental design and discussed the manuscript. M.H. and J.W. conceived and supervised the study, and revised the manuscript.

Funding
This work was supported by grants from the National Natural Science Foundation of China (No. 82203974, 81930090, U22A20279), the Natural Science Foundation of Chongqing City (No. CSTB2024NSCQ-JQX0002, CSTB2023NSCQ-MSX0284), Postdoctoral Innovative Talent Support Program of China (No. BX20220398).

Data availability
RNA-sequencing data have been uploaded to the Gene Expression Omnibus (GEO) database (no. GSE252894 and no. GSE281040).

Declarations

Competing interests
The authors declare no competing interests.

Conflict of interest
The authors declare no conflict of interest.

Received: 31 July 2024 / Accepted: 22 November 2024
Published online: 03 December 2024

References

1. Mitchell E, Spencer Chapman M, Williams N, Dawson KJ, Mende N, Calderbank EF, Jung H, Mitchell T, Coorens THH, Spencer DH, et al. Clonal dynamics of haematopoiesis across the human lifespan. Nature. 2022;606:343–50.
2. Pinho S, Frenette PS. Haematopoietic stem cell activity and interactions with the niche. Nat Rev Mol Cell Biol. 2019;20:303–20.
3. de Morree A, Rando TA. Regulation of adult stem cell quiescence and its functions in the maintenance of tissue integrity. Nat Rev Mol Cell Biol. 2023;24:334–54.
4. Hu M, Lu Y, Wang S, Zhang Z, Qi Y, Chen N, Shen M, Chen F, Chen M, Yang L, et al. CD63 acts as a functional marker in maintaining hematopoietic stem cell quiescence through supporting TGFbeta signaling in mice. Cell Death Differ. 2022;29:178–91.
5. Vanickova K, Milosevic M, Ribeiro Bas I, Burocziova M, Yokota A, Danek P, Grusanovic S, Chilinski M, Plewczynski D, Rohlena J, et al. Hematopoietic stem cells undergo a lymphoid to myeloid switch in early stages of emergency granulopoiesis. EMBO J. 2023;42:e113527.
6. Chen N, Quan Y, Chen M, Lu Y, Yang L, Wang S, Chen F, Xu Y, Shen M, Zeng H, et al. Melanocortin/MC5R axis regulates the proliferation of hematopoietic stem cells in mice after ionizing radiation injury. Blood Adv. 2023;7:3199–212.
7. Zhang Y, Roos M, Himburg H, Termini CM, Quarmyne M, Li M, Zhao L, Kan J, Fang T, Yan X, et al. PTPsigma inhibitors promote hematopoietic stem cell regeneration. Nat Commun. 2019;10:3667.
8. Wroblewski M, Scheller-Wendorff M, Udonta F, Bauer R, Schlichting J, Zhao L, Ben Batalla I, Gensch V, Pasler S, Wu L, et al. BET-inhibition by JQ1 promotes proliferation and self-renewal capacity of hematopoietic stem cells. Haematologica. 2018;103:939–48.
9. Shao L, Luo Y, Zhou D. Hematopoietic stem cell injury induced by ionizing radiation. Antioxid Redox Signal. 2014;20:1447–62.
10. Hu L, Yin X, Zhang Y, Pang A, Xie X, Yang S, Zhu C, Li Y, Zhang B, Huang Y, et al. Radiation-induced bystander effects impair transplanted human hematopoietic stem cells via oxidative DNA damage. Blood. 2021;137:3339–50.
11. Kuramoto K, Liang H, Hong JH, He C. Exercise-activated hepatic autophagy via the FN1-alpha5beta1 integrin pathway drives metabolic benefits of exercise. Cell Metab. 2023;35:620–e632625.
12. Smith JAB, Murach KA, Dyar KA, Zierath JR. Exercise metabolism and adaptation in skeletal muscle. Nat Rev Mol Cell Biol. 2023;24:607–32.
13. Hawley JA, Hargreaves M, Joyner MJ, Zierath JR. Integrative biology of exercise. Cell. 2014;159:738–49.
14. Liu L, Kim S, Buckley MT, Reyes JM, Kang J, Tian L, Wang M, Lieu A, Mao M, Rodriguez-Mateo C, et al. Exercise reprograms the inflammatory landscape of multiple stem cell compartments during mammalian aging. Cell Stem Cell. 2023;30:689–e705684.
15. Baker JM, De Lisio M, Parise G. Endurance exercise training promotes medullary hematopoiesis. FASEB J. 2011;25:4348–57.
16. De Lisio M, Parise G. Characterization of the effects of exercise training on hematopoietic stem cell quantity and function. J Appl Physiol (1985). 2012;113:1576–84.
17. Ho TT, Dellorusso PV, Verovskaya EV, Bakker ST, Flach J, Smith LK, Ventura PB, Lansinger OM, Herault A, Zhang SY, et al. Aged hematopoietic stem cells are refractory to bloodborne systemic rejuvenation interventions. J Exp Med. 2021;218:e20210223.
18. Fiuza-Luces C, Valenzuela PL, Galvez BG, Ramirez M, Lopez-Soto A, Simpson RJ, Lucia A. The effect of physical exercise on anticancer immunity. Nat Rev Immunol. 2024;24:282–93.
19. Frodermann V, Rohde D, Courties G, Severe N, Schloss MJ, Amatullah H, McAlpine CS, Cremer S, Hoyer FF, Ji F, et al. Exercise reduces inflammatory cell production and cardiovascular inflammation via instruction of hematopoietic progenitor cells. Nat Med. 2019;25:1761–71.
20. Kim DS, Weber T, Straube U, Hellweg CE, Nasser M, Green DA, Fogtman A. The potential of Physical Exercise to Mitigate Radiation Damage-A systematic review. Front Med (Lausanne). 2021;8:585483.
21. De Lisio M, Phan N, Boreham DR, Parise G. Exercise-induced protection of bone marrow cells following exposure to radiation. Appl Physiol Nutr Metab. 2011;36:80–7.
22. Emmons R, Ngu M, Xu G, Hernandez-Saavedra D, Chen H. Effects of obesity and Exercise on Bone Marrow Progenitor cells after Radiation. Med Sci Sports Exerc. 2019;51:1126–36.
23. Dietlein N, Rodewald HR. Runner's niche: multipurpose stromal cells maintained by exercise. Trends Immunol. 2021;42:841–3.
24. Severinsen MCK, Pedersen BK. Muscle-organ crosstalk: the emerging roles of Myokines. Endocr Rev. 2020;41:594–609.
25. Hu M, Lu Y, Zeng H, Zhang Z, Chen S, Qi Y, Xu Y, Chen F, Tang Y, Chen M, et al. MicroRNA-21 maintains hematopoietic stem cell homeostasis through sustaining the NF-kappaB signaling pathway in mice. Haematologica. 2021;106:412–23.
26. Hu M, Zeng H, Chen S, Xu Y, Wang S, Tang Y, Wang X, Du C, Shen M, Chen F, et al. SRC-3 is involved in maintaining hematopoietic stem cell quiescence by regulation of mitochondrial metabolism in mice. Blood. 2018;132:911–23.
27. Hu M, Chen N, Chen M, Chen F, Lu Y, Xu Y, Yang L, Zeng H, Shen M, Chen X, et al. Transcription factor Nkx2-3 maintains the self-renewal of hematopoietic stem cells by regulating mitophagy. Leukemia. 2023;37:1361–74.
28. Anderson EJ, Vistoli G, Katunga LA, Funai K, Regazzoni L, Monroe TB, Gilardoni E, Cannizzaro L, Colzani M, De Maddis D, et al. A carnosine analog mitigates metabolic disorders of obesity by reducing carbonyl stress. J Clin Invest. 2018;128:5280–93.
29. Shao L, Feng W, Li H, Gardner D, Luo Y, Wang Y, Liu L, Meng A, Sharpless NE, Zhou D. Total body irradiation causes long-term mouse BM injury via induction of HSC premature senescence in an Ink4a- and arf-independent manner. Blood. 2014;123:3105–15.
30. Chang J, Wang Y, Shao L, Laberge RM, Demaria M, Campisi J, Janakiraman K, Sharpless NE, Ding S, Feng W, et al. Clearance of senescent cells by ABT263 rejuvenates aged hematopoietic stem cells in mice. Nat Med. 2016;22:78–83.
31. Suo M, Rommelfanger MK, Chen Y, Amro EM, Han B, Chen Z, Szafranski K, Chakkarappan SR, Boehm BO, MacLean AL, Rudolph KL. Age-dependent effects of Igf2bp2 on gene regulation, function, and aging of hematopoietic stem cells in mice. Blood. 2022;139:2653–65.
32. Bogeska R, Mikecin AM, Kaschutnig P, Fawaz M, Buchler-Schaff M, Le D, Ganuza M, Vollmer A, Paffenholz SV, Asada N, et al. Inflammatory exposure drives long-lived impairment of hematopoietic stem cell self-renewal activity and accelerated aging. Cell Stem Cell. 2022;29:1273–e12841278.
33. Everaert I, De Naeyer H, Taes Y, Derave W. Gene expression of carnosine-related enzymes and transporters in skeletal muscle. Eur J Appl Physiol. 2013;113:1169–79.
34. Boldyrev AA, Aldini G, Derave W. Physiology and pathophysiology of carnosine. Physiol Rev. 2013;93:1803–45.
35. Guney Y, Turkcu UO, Hicsonmez A, Andrieu MN, Guney HZ, Bilgihan A, Kurtman C. Carnosine may reduce lung injury caused by radiation therapy. Med Hypotheses. 2006;66:957–9.
36. Haeri SA, Rajabi H, Fazelipour S, Hosseinimehr SJ. Carnosine mitigates apoptosis and protects testicular seminiferous tubules from gamma-radiation-induced injury in mice. Andrologia. 2014;46:1041–6.
37. Van der Stede T, Spaas J, de Jager S, De Brandt J, Hansen C, Stautemas J, Vercammen B, De Baere S, Croubels S, Van Assche CH, et al. Extensive profiling of histidine-containing dipeptides reveals species- and tissue-specific distribution and metabolism in mice, rats, and humans. Acta Physiol (Oxf). 2023;239:e14020.
38. Nagai K, Tanida M, Niijima A, Tsuruoka N, Kiso Y, Horii Y, Shen J, Okumura N. Role of L-carnosine in the control of blood glucose, blood pressure, thermogenesis, and lipolysis by autonomic nerves in rats: involvement of the circadian clock and histamine. Amino Acids. 2012;43:97–109.
39. Yan R, Zhang P, Shen S, Zeng Y, Wang T, Chen Z, Ma W, Feng J, Suo C, Zhang T, et al. Carnosine regulation of intracellular pH homeostasis promotes lysosome-dependent tumor immunoevasion. Nat Immunol. 2024;25:483–95.
40. Matthews JJ, Artioli GG, Turner MD, Sale C. The physiological roles of carnosine and beta-alanine in exercising human skeletal muscle. Med Sci Sports Exerc. 2019;51:2098–108.
41. Shao L, Sun Y, Zhang Z, Feng W, Gao Y, Cai Z, Wang ZZ, Look AT, Wu WS. Deletion of proapoptotic Puma selectively protects hematopoietic stem and progenitor cells against high-dose radiation. Blood. 2010;115:4707–14.
42. Belle JI, Petrov JC, Langlais D, Robert F, Cencic R, Shen S, Pelletier J, Gros P, Nijnik A. Repression of p53-target gene Bbc3/PUMA by MYSM1 is essential for the survival of hematopoietic multipotent progenitors and contributes to stem cell maintenance. Cell Death Differ. 2016;23:759–75.
43. Chen J, Ren C, Yao C, Baruscotti M, Wang Y, Zhao L. Identification of the natural chalcone glycoside hydroxysafflor yellow A as a suppressor of P53 overactivation-associated hematopoietic defects. MedComm (2020). 2023;4:e352.
44. Wang M, Brandt LTL, Wang X, Russell H, Mitchell E, Kamimae-Lanning AN, Brown JM, Dingler FA, Garaycoechea JI, Isobe T, et al. Genotoxic aldehyde stress prematurely ages hematopoietic stem cells in a p53-driven manner. Mol Cell. 2023;83:2417–e24332417.
45. Mouraret N, Marcos E, Abid S, Gary-Bobo G, Saker M, Houssaini A, Dubois-Rande JL, Boyer L, Boczkowski J, Derumeaux G, et al. Activation of lung p53

by Nutlin-3a prevents and reverses experimental pulmonary hypertension. Circulation. 2013;127:1664–76.
46. Leonova KI, Shneyder J, Antoch MP, Toshkov IA, Novototskaya LR, Komarov PG, Komarova EA, Gudkov AV. A small molecule inhibitor of p53 stimulates amplification of hematopoietic stem cells but does not promote tumor development in mice. Cell Cycle. 2010;9:1434–43.
47. Termini CM, Pang A, Fang T, Roos M, Chang VY, Zhang Y, Setiawan NJ, Signaevskaia L, Li M, Kim MM, et al. Neuropilin 1 regulates bone marrow vascular regeneration and hematopoietic reconstitution. Nat Commun. 2021;12:6990.
48. Acharya SS, Fendler W, Watson J, Hamilton A, Pan Y, Gaudiano E, Moskwa P, Bhanja P, Saha S, Guha C, et al. Serum microRNAs are early indicators of survival after radiation-induced hematopoietic injury. Sci Transl Med. 2015;7:287ra269.
49. Mahootchi E, Cannon Homaei S, Kleppe R, Winge I, Hegvik TA, Megias-Perez R, Totland C, Mogavero F, Baumann A, Glennon JC, et al. GADL1 is a multifunctional decarboxylase with tissue-specific roles in beta-alanine and carnosine production. Sci Adv. 2020;6:eabb3713.
50. Xu M, He RR, Zhai YJ, Abe K, Kurihara H. Effects of carnosine on cyclophosphamide-induced hematopoietic suppression in mice. Am J Chin Med. 2014;42:131–42.
51. Deng J, Zhong YF, Wu YP, Luo Z, Sun YM, Wang GE, Kurihara H, Li YF, He RR. Carnosine attenuates cyclophosphamide-induced bone marrow suppression by reducing oxidative DNA damage. Redox Biol. 2018;14:1–6.
52. Caruso G, Caraci F, Jolivet RB. Pivotal role of carnosine in the modulation of brain cells activity: Multimodal mechanism of action and therapeutic potential in neurodegenerative disorders. Prog Neurobiol. 2019;175:35–53.
53. Banerjee S, Poddar MK. Carnosine research in relation to aging brain and neurodegeneration: a blessing for geriatrics and their neuronal disorders. Arch Gerontol Geriatr. 2020;91:104239.
54. Solana-Manrique C, Sanz FJ, Martinez-Carrion G, Paricio N. Antioxidant and neuroprotective effects of Carnosine: therapeutic implications in neurodegenerative diseases. Antioxid (Basel). 2022;11:848.
55. Mak MK, Wong-Yu IS, Shen X, Chung CL. Long-term effects of exercise and physical therapy in people with Parkinson disease. Nat Rev Neurol. 2017;13:689–703.
56. Martinez MW, Kim JH, Shah AB, Phelan D, Emery MS, Wasfy MM, Fernandez AB, Bunch TJ, Dean P, Danielian A, et al. Exercise-Induced Cardiovascular adaptations and Approach to Exercise and Cardiovascular Disease: JACC State-of-the-art review. J Am Coll Cardiol. 2021;78:1453–70.
57. Liu XQ, Jiang L, Lei L, Nie ZY, Zhu W, Wang S, Zeng HX, Zhang SQ, Zhang Q, Yard B, Wu YG. Carnosine alleviates diabetic nephropathy by targeting GNMT, a key enzyme mediating renal inflammation and fibrosis. Clin Sci (Lond). 2020;134:3175–93.
58. Hwang B, Shin SS, Song JH, Choi YH, Kim WJ, Moon SK. Carnosine exerts antitumor activity against bladder cancers in vitro and in vivo via suppression of angiogenesis. J Nutr Biochem. 2019;74:108230.
59. Qi Y, Chen S, Lu Y, Zhang Z, Wang S, Chen N, Shen M, Chen F, Chen M, Quan Y, et al. Grape seed proanthocyanidin extract ameliorates ionizing radiation-induced hematopoietic stem progenitor cell injury by regulating Foxo1 in mice. Free Radic Biol Med. 2021;174:144–56.
60. Li W, Wang X, Dong Y, Huo Q, Yue T, Wu X, Lu L, Zhang J, Zhao Y, Dong H, Li D. Nicotinamide riboside intervention alleviates hematopoietic system injury of ionizing radiation-induced premature aging mice. Aging Cell. 2023;22:e13976.
61. Xu G, Wu H, Zhang J, Li D, Wang Y, Wang Y, Zhang H, Lu L, Li C, Huang S, et al. Metformin ameliorates ionizing irradiation-induced long-term hematopoietic stem cell injury in mice. Free Radic Biol Med. 2015;87:15–25.

Publisher's note